

A deep Aurum reservoir: Stable compounds of two bulk-immiscible metals under pressure

Adebayo A. Adeleke^{a,b,e}, Stanimir A. Bonev^{b,1}, Christine J. Wu^b, Ericmoore E. Jossou^{c,d}, and Erin R. Johnson^{e,1}

^aDepartment of Physics and Engineering Physics, University of Saskatchewan, Saskatoon, Saskatchewan S7N 5E2, Canada; ^bQuantum Simulation Group, Materials Science Division, Lawrence Livermore National Laboratory, Livermore, California 94550, USA; ^cDepartment of Mechanical Engineering, University of Saskatchewan, Saskatoon, Saskatchewan S7N 5A9, Canada; ^dNuclear Science & Technology Department, Brookhaven National Laboratory, Upton, New York 11973, USA; ^eDepartment of Chemistry, Dalhousie University, Halifax, Nova Scotia B3H 4R2, Canada

This manuscript was compiled on September 14, 2022

The Earth's crust is known to be depleted of gold, among other slightly heavy noble metals transported by magma from the Earth's mantle to the crust. The bulk silicate Earth (BSE) model also suggests significant depletion of Au in the silicate mantle itself, which cannot be explained by the amount of Au in the mantle's magma. This implies that Au could remain in the lower mantle and form stable compounds, especially with iron, which is the predominant element within the core. While Fe does not form binary compounds or a bulk alloy with Au under ambient conditions, it may do so at the elevated pressures found in the Earth's interior. Here, using density-functional methods, we investigated the possibility of identifying stable, binary Fe-Au compounds at pressures up to 210 GPa. We found three such Fe-Au compounds, which are stabilized by pressure and notable electron transfer, including an orthorhombic AuFe₄ phase that is ferromagnetic in nature with Au possessing a significant magnetic moment. While our results suggest that thermal convection due to the conductivities and the heat flux from the Fe-Au compounds could be an energy source to power the Earth's geodynamo, they also point towards changes in Au's chemical properties, as it can exist as either an anion or cation under pressure. In addition, the sound velocity and the density predicted for the various Fe-Au compounds suggest that they could shed light on the composition of the core-mantle boundary and the Earth's core, while demonstrating how the presence of trace amounts of Au could influence agreement with seismic data.

Gold | Intermetallic compound | Earth's interior | Iron

Segregation of the proto-Earth's iron-rich core from its surrounding silicate, and collision-induced aggregation of planetesimals, resulted in the formation of the Earth within a period of 30-40 million years (1). Geological and seismological models for various regions of the Earth are constrained through comparisons with the composition of meteorites, which are similar to the planetesimals that helped form our planet (2). These direct comparisons have led to the conclusion that the Earth's crust was depleted of some siderophile elements, such as nickel, platinum, and gold. Lithophiles (with pressure-induced siderophilic properties), such as vanadium, chromium, manganese, and cesium, may have also percolated into the silicate mantle and the Earth's core (3, 4). Thus, the composition of the silicate mantle is expanded to include Cs, Ni, Pt, Au, V, Cr and Mn (4-6).

Of these elements, Au is of particular interest because of its economic value (7), inertness (8), and the remarkable stability of its crystal structure over a wide range of pressures traversing that of the Earth's core (9-13). In addition to depletion of Au from the Earth's crust, the bulk silicate Earth (BSE) model also suggests significant depletion of Au from the silicate

mantle, which cannot be explained by the amount of Au in the mantle's magma (1). Since Au is heavy and less volatile than Cr, V, and Mn (1, 14), it could not have evaporated into space. However, it is challenging to propose a likely form for Au in the neighborhood of the core-mantle boundary (CMB) without violating various constraints imposed in seismological models (15, 16) of the Earth. A possible solution was proposed by Wood and coworkers (17), who suggested that the Au further percolated into the Earth's iron-rich core.

Meanwhile, seismological studies (18) indicate a 2-5% density deficit for the Earth's solid inner core, proposing that the core is not a 'bank' of pure Fe after all. The core must, therefore, be home to some light siderophile elements, such as H, C, Si, S, and K (19-22). Additionally, experiments at elevated temperatures and pressures, combined with theoretical studies, suggest the reactivity of the noble gases Xe (23) and Ar (24) with Ni and Fe. The stability of the resulting compounds was attributed to pressure-induced energy raising of the valence p-shell states of the noble gas, allowing charge transfer to the partially filled 3d or 4s states of the transition metal (23). However, none of these studies could exhaustively explain the mass and density deficit in the Earth's core from the preliminary reference Earth model (PREM) (15). This means that slightly heavy (siderophile) metals depleted in the Earth's crust could have found their way into the core, where they form stable compounds (3). Thus, knowing the form(s) in which Au could exist when subject to the thermodynamic

Significance Statement

We have demonstrated that gold (Au), a noble and precious metal, can react with hexagonal close packed iron (Fe) to form stable intermetallic compounds under sufficient compression. We also demonstrated that Au, which is diamagnetic at ambient pressure, could attain a magnetic moment in compound form when compressed to the pressures found in the Earth's interior. The Fe-Au compounds show significant lattice thermal conductivities and their sound velocities have better agreement with seismic data relative to some other available binary models of the Earth's core. Our results suggest that the Earth's core could hold more Au than previously thought.

S.A.B. and A.A.A. designed research; A.A.A. performed research; E.E.J. and A.A.A. performed thermal conductivity calculations; A.A.A., S.A.B., C.J.W., E.E.J. and E.R.J. analyzed data; A.A.A. wrote the initial draft of the paper; A.A.A., S.A.B. and E.R.J. wrote the advanced version of the paper with contribution from all authors; S.A.B., C.J.W. and E.R.J. contributed funding and computer resources; S.A.B., C.J.W. and E.R.J. supervised research.

The authors declare no conflicting interest.

¹To whom correspondence should be addressed. E-mail: S.A.B.: bonev2@llnl.gov; E.R.J.: erin.johnson@dal.ca

Table 1. Structural parameters (and Bader atomic charges) of various predicted Fe-Au phases at 0 K

System	P (GPa)	SG	Lattice parameter	Element	Wyc. site	Atomic coordinate (fractional)	Bader charge/atom
AuFe ₄	140	Cmcm	a = 12.12 Å, b = 4.00 Å, c = 3.69 Å	Au	4c	0.000, 0.796, 0.750	0.34
				Fe	8g	0.883, 0.325, 0.750	0.33 / 0.37
				Fe	8g	0.705, 0.333, 0.750	-0.51 / -0.53
AuFe ₄	200	I4/m	a = 10.00 Å, c = 10.01 Å	Au	2b	0.000, 0.000, 0.500	0.40
				Fe	8h	0.091, 0.690, 0.000	-0.10
AuFe ₃	200	Pmmn	a = 2.35 Å, b = 2.95 Å, c = 9.86 Å	Au	2b	0.000, 0.500, 0.585	-0.26
				Fe	2b	0.000, 0.500, 0.833	0.04
				Fe	2b	0.500, 0.000, 0.947	0.03 / 0.04
				Fe	2b	0.500, 0.000, 0.729	0.18 / 0.19

conditions present within the core may help provide a solution to the problem of depleted Au.

It is well known that the Earth's core is predominantly composed of Fe (4, 15, 19). Thus, a natural line of thought would be that Au, which was drawn towards and into the core, may have formed a bimetallic compound with Fe. However, under ambient conditions, the magnetic metals (Fe, Co, and Ni) do not form compounds or bulk alloys with many heavier metals, including Au. This is primarily because of the size mismatch between the constituent atoms, coupled with little or no solid solubility (25, 26). If a stable, binary Fe-Au compound is demonstrated to form under high pressures, transversing that of the Earth's interior, we can then begin to search for Au in this form within the mantle and core.

To this end, we explore the Fe-Au potential energy surface from ambient to high pressure using density-functional theory (DFT). Interesting physics plays out under pressure and, as such, ushers in new chemistry (27). This is exemplified by the predicted formation of stable intermetallic compounds of Fe and Au under high pressure, reported here for the first time. Analysis of the electron density (28) reveals an unusual charge transfer between Au and Fe. Using a combination of DFT and the Boltzmann transport equation, we also predict the phonon-assisted thermal conductivity of the Fe-Au compounds at thermodynamic conditions relevant to the lower mantle (near the CMB) and the outer core. This work contributes to our understanding of the Earth's lower mantle and the outer core, revealing how it is able to keep such a noble metal as Au mixed with Fe without decomposition into its elemental form.

RESULTS

Phase stability and stable crystal structures of Fe-Au. We systematically searched for stable structures of the binary compounds Fe_xAu_y ($x, y \in \{1 \dots 4\}$) with cells containing 1-4 structural formula units at 0 K temperature and pressures ranging from 0-200 GPa. Spin-polarized calculations were carried out on the lowest-energy structures for all stoichiometries explored and the nonmagnetic configurations were found to be the most energetically favorable, with an exception observed for the AuFe₄ stoichiometry at 140 GPa.

The convex hull calculated at various search pressures shows that Au and Fe do not form any stable binary compounds at ambient conditions up to 140 GPa (Fig. 1). At this pressure, an orthorhombic AuFe₄ phase (with space group Cmcm) becomes thermodynamically stable relative to elemental fcc-Au and hcp-Fe (see Fig. 1a) and, as such, should be synthesizable.

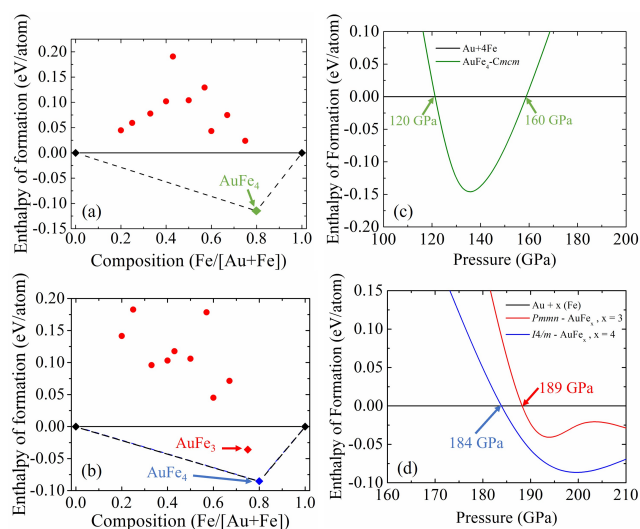


Fig. 1. (color online) Calculated cold enthalpy ($U+pV$) of formation (0 K) of various Fe-Au compounds with respect to constituent elemental decomposition (a) at 140 GPa (b) at 200 GPa. Calculated enthalpies per atom for (c) Cmcm-AuFe₄ structure with respect to the mixture of elemental Fe and Au (d) Pmmn-AuFe₃ and I4/m-AuFe₄ structures with respect to the mixture of elemental Fe and Au.

Furthermore, at 200 GPa, AuFe₄ crystallizes into a tetragonal cell with space group I4/m. An orthorhombic AuFe₃ phase (space group Pmmn) that is metastable with respect to the tetragonal I4/m-AuFe₄ was also uncovered (see Fig. 1b). Inclusion of the free-energy contribution from lattice vibrations at 0 K (zero-point energy, ZPE) did not stabilize the formation pressure, nor stabilize other phases that were not initially energetically favorable. However, the magnitude of the formation enthalpy (enthalpy being $U+pV$) for the stable phases were slightly changed (Fig. S1).

The calculated equations of states (EOS) for the predicted structures reveal that the Cmcm-AuFe₄ has a stability pressure range of 120-160 GPa (Fig. 1c) and, as such, will decompose below 120 GPa and above 160 GPa. This explains why our structure searches at 100 GPa and 200 GPa could not find this structure. On the other hand, the I4/m-AuFe₄ and Pmmn-AuFe₃ phases are thermodynamically stable from 184 and 189 GPa, respectively, up to at least 210 GPa (Fig. 1d).

Structural geometry of Fe-Au phases. The structural parameters of the thermodynamically stable phases of the Fe_xAu_y compounds are presented in Table 1 and the unit-cell ge-

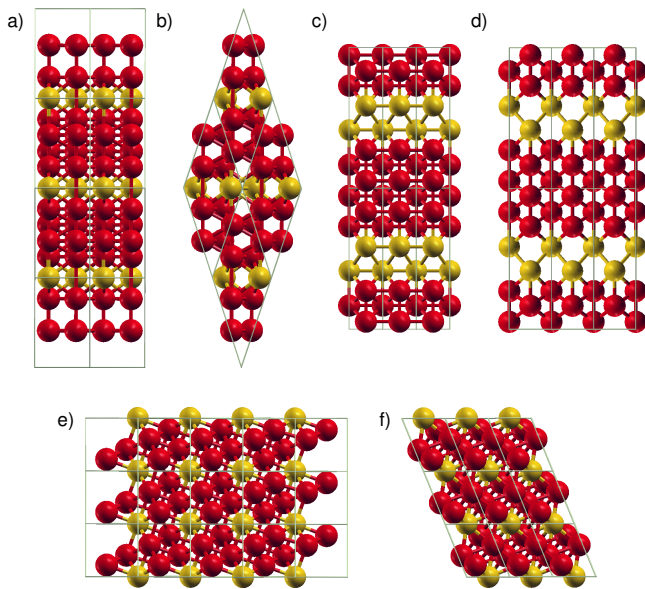


Fig. 2. (color online) Crystal structures of Cmcm-AuFe₄ at 140 GPa (a,b), Pmmn-AuFe₃ at 200 GPa (c,d), and I4/m-AuFe₄ at 200 GPa (e,f). Two views are shown for each crystal.

ometries are shown in Figure 2. The Cmcm-AuFe₄ phase at 140 GPa is characterized by layers of distorted hexagonal-close-packed Fe atoms connected by a layer of Au atoms (Fig. 2a,b). This leads to two distinct Fe environments – those closest to the Au and those in the interior of the Fe layer. As we will see, the presence of two distinct Fe environments facilitates charge transfer. The Fe-Au bond lengths range from 2.34-2.53 Å, the Au-Au bonds are 2.45 Å, and the Fe-Fe bonds range from 2.16-2.30 Å (compared to 2.21 Å for hcp-Fe at 140 GPa).

Metastable Pmmn-AuFe₃ at 200 GPa has a phase-separated, layered structure. Six rows of Fe atoms form a hexagonal-close-packed arrangement, separated by a double layer of Au atoms (Fig. 2c,d) stacked along the *c* direction. This leads to three distinct Fe environments that vary by their proximity to the Au layer. The Fe-Au bond lengths are 2.36 and 2.47 Å, while the Au-Au bond lengths are 2.35 Å and the Fe-Fe bond lengths range from 2.15-2.35 Å.

In the I4/m-AuFe₄ structure at 200 GPa, Au atoms adopt body-centred-cubic positions, forming bonds with 12 symmetry-equivalent Fe atoms at the midpoints of each side of the surrounding cube (Fig. 2e). The Fe-Au bond length is 2.29 Å, which is shorter than that observed in the other two crystals, and therefore stronger if we follow the ‘shorter = stronger’ maxim for chemical bonds. The Fe-Fe bond lengths range from 2.14-2.35 Å and there are no Au-Au bonds in this structure.

Magnetic properties of Fe-Au phases. We performed spin-polarized calculations on the Cmcm-AuFe₄ phase at 140 GPa, and on $2 \times 2 \times 2$ supercells of the Pmmn-AuFe₃ and I4/m-AuFe₄ phases at 200 GPa. The results reveal that the ferromagnetic configuration, with a magnetic moment of $2.15\mu_B$, is the ground state for Cmcm-AuFe₄. This ferromagnetic configuration is 0.4 meV/atom lower in energy than the nonmagnetic configuration and ~ 0.17 eV/atom lower in energy than the paramagnetic, antiferromagnetic, and ferrimagnetic configurations. While elemental gold exists as a diamagnet in bulk

form (29), our results indicate that gold can adopt an induced ferromagnetic moment (of $0.52\mu_B$ in this case) when placed in the ferromagnetic environment of the surrounding iron. This is consistent with previous findings for other materials (30–33).

Conversely, the nonmagnetic configuration is preferred for both Pmmn-AuFe₃ and I4/m-AuFe₄ at 200 GPa. For both of these phases, the formation energy is 1.2 meV/atom lower than the ferromagnetic case and 0.2 eV/atom lower than the paramagnetic, antiferromagnetic, and ferrimagnetic configurations. This is not surprising since 200 GPa already exceeds the magnetic transition pressure for most transition metals (34).

Electronic structure of Fe-Au phases. The calculated electronic band structures (Fig. S5) show that all the three Fe-Au systems reported in this work are metallic. The electronic densities of states (DOS) projected to orbitals (Fig. 3) reveal that the states in the vicinity of the Fermi energy level are primarily Fe 3d states, with some contribution from Au 5d states. This implies that the Fe 3d and Au 5d states are responsible for the metallicity of the phases reported here.

The results of Bader charge analysis are shown in Tables 1 and S2, as well as Fig. S3. The observed atomic charges vary significantly between the three phases and, even within a given material, are highly dependent on the coordination environments. As expected from its greater electronegativity, Au acts as anion in the metastable Pmmn-AuFe₃ phase at 200 GPa, with each Au atom gaining 0.26e⁻ and the Fe atoms at the edges of the Fe layers losing 0.19e⁻. The Fe atoms in the interior of the layers have greatly reduced partial charges of 0.03 and 0.04e⁻. A similar negative oxidation state in Au was reported for caesium auride (CsAu) (35, 36).

Conversely, for I4/m-AuFe₄ at 200 GPa, each Au atom lies at the center of the unit cell and is coordinated to 12 Fe atoms, in a geometry similar to what is observed in the ionic lattices of some actinide complexes such as [Th(NO₃)₆]²⁻ (37). Here, each Au atom is cationic, losing 0.40e⁻, while each Fe atom gains 0.10e⁻, making them anionic. Fe is known to become highly electronegative at such high pressures and a similar charge-transfer mechanism has been reported for Fe and Ni in the Xe-Fe/Ni system (23).

Finally, for Cmcm-AuFe₄ at 140 GPa, the Au atoms each lose 0.34e⁻, again making them cationic. However, the two distinct Fe environments in the crystal have very different atomic charges, similar to what was reported in α -Mn (38). The Fe atoms at the first 8g sites directly bonded to the Au are also cationic and lose between 0.33e⁻ and 0.37e⁻. Since they have comparable charges to the Au atoms, we will refer to these Fe atoms as pseudo-Au atoms. The Fe atoms at the second 8g sites (in the interior of the Fe layer) gain between 0.51e⁻ and 0.53e⁻ each to become anions. Therefore, the Cmcm-AuFe₄ phase is stabilized through electron transfer from Au and pseudo-Au atoms to Fe atoms to give regions of alternating charge.

Dynamic, mechanical, and thermal properties of Fe-Au phases. We established the dynamic stability of the various predicted phases of Fe-Au through the calculation of phonon dispersion relations (Fig. 4 a-c). All three show no imaginary frequencies throughout the BZ, indicating dynamic stability within the harmonic approximation. We further investigated the response of the three predicted phases to external strain

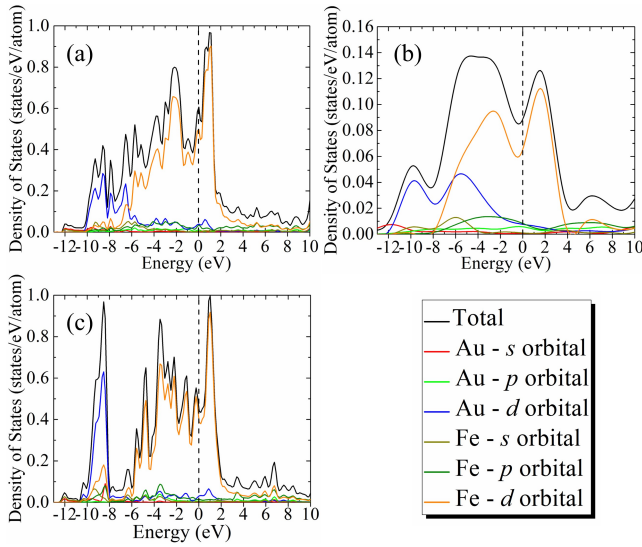


Fig. 3. (color online) Calculated electronic density of states projected to orbitals for (a) Cmcm-AuFe₄ at 140 GPa, (b) Pmmn-AuFe₃ at 200 GPa, and (c) I4/m-AuFe₄ at 200 GPa. The black dashed line represents the Fermi energy level.

(39–41) which, in principle, is a measure of their elastic and mechanical stability (Table S1). The results indicate that all the predicted phases are elastically and mechanically stable and their Pugh’s ratio (42) also indicates that they are ductile.

At 200 GPa, two structures are predicted to be synthesizable (Fig. 1b) with the I4/m-AuFe₄ phase being the thermodynamic ground state and the Pmmn-AuFe₃ phase being metastable. With an enthalpy difference of only ~40 meV/atom between I4/m-AuFe₄ and the combination of the Pmmn-AuFe₃ phase and hcp-Fe, differences in their vibrational free energies at high temperature could compensate for the enthalpy difference and reverse the stability ranking. Therefore, we calculated the Helmholtz free-energy evolution with temperature (T) at fixed volume (V) for both phases at 200 GPa within the harmonic approximation (Fig. 4d). The vibrational free-energy contribution is (43)

$$F_{vib}(T) = \frac{1}{2} \sum_{\omega} g(\omega) \hbar \omega + k_B T \sum_{\omega} g(\omega) \ln \left[1 - \exp \left(-\frac{\hbar \omega}{k_B T} \right) \right], \quad [1]$$

where $g(\omega)$ is the normalized density of states (phDOS) for the phonon branch ω and k_B is Boltzmann’s constant.

The calculated temperature evolution of the relative free energies (Fig. 4d) reveals that I4/m-AuFe₄ is preferred at ambient temperature up to ~1750 K. Between 1750 K and 2000 K, the two phases are effectively degenerate, while Pmmn-AuFe₃ + hcp-Fe becomes preferable at high temperatures above 2000 K. This preference can be motivated by the presence of more low-frequency phonons (<4 THz) for Pmmn-AuFe₃ (Fig. 4b) compared to I4/m-AuFe₄ (Fig. 4c), which will have a greater contribution to the vibrational entropy. The latent heat absorbed in the I4/m-AuFe₄ → Pmmn-AuFe₃ + hcp-Fe transition at 2000 K is estimated from the vibrational entropy to be 0.025 eV/atom (Fig. S9). The experimental implication of this observation is that the metastable Pmmn-AuFe₃ phase could potentially be prepared by laser-heating a compressed mixture of Au and Fe (with a molar ratio consistent with the stoichiometry) above 2000 K.

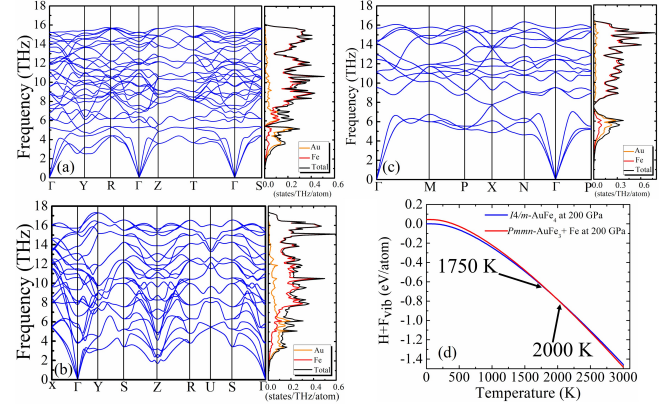


Fig. 4. (color online) Phonon dispersion relations for (a) Cmcm-AuFe₄ at 140 GPa, (b) Pmmn-AuFe₃ at 200 GPa, and (c) I4/m-AuFe₄ at 200 GPa. Also shown is (d) the relative free energies of I4/m-AuFe₄ and Pmmn-AuFe₃ + hcp-Fe at 200 GPa as a function of temperature. The I4/m-AuFe₄ structure at 0 K was used as the zero of energy.

Thermal conductivity of Fe-Au. The thermal conductivity of solids is governed by the phonon vibrations, coupled with the scattering processes they encounter. During structural phase transitions driven by soft phonons, the phonon-assisted thermal conductivity is expected to be strongly modified, since the soft mode will experience a frequency and group velocity shift, which will in turn modify the allowed phonon scattering processes in the system. The modification of phonon modes also has significant implications for heat transport.

We computed the thermal conductivity of the three predicted Fe-Au intermetallic compounds by solving the Boltzmann transport equation (BTE) for a range of temperatures. The results are shown in Fig. 5a and highlight the significant effect of phase change on the thermal conductivity of these compounds. While the relaxation time approximation (RTA) usually underestimates the thermal conductivity (since it treats both Normal and Umklapp scattering as resistive processes (44)), we found that the RTA produces results within 0.5% of the iterative solution for all three phases at room temperature.

In the analysis of measured data, some (45) have concluded that the acoustic modes dominate thermal transport and that the optical modes contribute negligibly due to low group velocities. However, we have found that this assumption cannot explain the comparatively large thermal conductivity (k_{ph}) values for the Fe-Au systems studied in this work. From Fig. 4a-c, there is no gap between the acoustic and optical modes in the phonon dispersion in either Cmcm-AuFe₄ or Pmmn-AuFe₃ at 200 GPa, while a small gap exists for I4/m-AuFe₄. Such gaps are often attributed to atomic mass differences and can suppress the interaction of acoustic phonons with optical phonons above the gap (46). To investigate further, we examined the contributions of each phonon mode from our BTE solution as shown in Fig. 5c and Fig. S4. At 300 K (Fig. S4), optical phonon modes contribute 51% of the total k_{ph} of Pmmn-AuFe₃, while the contribution is 20% and 43% for Cmcm-AuFe₄ and I4/m-AuFe₄, respectively. At 2500 K (Fig. 5c), their contribution increases for all three phases, to 56%, 32%, and 54% for Pmmn-AuFe₃, Cmcm-AuFe₄, and I4/m-AuFe₄, respectively. This observation is consistent with the trend predicted from the group velocity (v_g) for acoustic

Table 2. Calculated sound speed (v_s) and density at 200 GPa and 0 K for Pmmn-AuFe₃ and I4/m-AuFe₄ compared with simulation data (48) of inner Earth's core model at 360 GPa and the PREM (15) data at 200 GPa.

System	Pmmn-AuFe ₃	I4/m-AuFe ₄	hcp-Fe	Fe ₆₂ C ₂	Fe ₆₀ C ₄	PREM
v_s (km/s)	4.28	4.82	6.80	6.38	6.0	3.6
Density (g/cm ³)	17.72	16.88	14.25	14.10	13.82	13

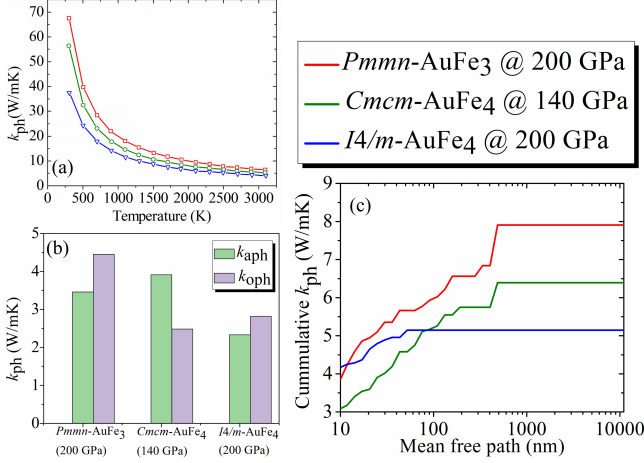


Fig. 5. (color online) (a) Calculated lattice thermal conductivity (k_{ph}) of the three Au-Fe phases as a function of temperature, ranging from 300 to 3100 K. (b) Decomposition of the k_{ph} of Au-Fe phases at 2500 K into contributions from the acoustic (k_{aph}) and optical (k_{oph}) modes. (c) Cumulative lattice thermal conductivity of Cmcm-AuFe₄ (140 GPa), Pmmn-AuFe₃ (200 GPa), and I4/m-AuFe₄ (200 GPa) as a function of the phonon mean-free-path at 2500 K.

modes, which would not support higher k_{ph} without other contributions. The high contributions from the optical modes are not surprising as similar contributions have been found in many complex materials (47). One reason for the strong optical phonon contribution may be due to the hybridization of low-energy optical modes with the acoustic modes. This causes a flattening of the acoustic dispersion for states away from the zone center (Fig. 4) and, therefore, a reduction in v_g , leading to reduced thermal transport from the acoustic phonons.

To determine the length scales for thermal transport, the cumulative k_{ph} with respect to the phonon mean free path is shown in Fig. 5b for the three phases of Au-Fe at 2500 K. This is informative for determining the length scales at which the phonons of each phase become relevant for heat conduction. Clearly, the I4/m-AuFe₄ phase is more sensitive to nano structuring compared to Pmmn-AuFe₃ and Cmcm-AuFe₄. This can be seen from the fact that the I4/m-AuFe₄ requires the least mean free path (< 100nm) to achieve its maximum, but the lowest lattice thermal conductivity and, as such, will transport heat more slowly.

DISCUSSION

Insight from elastic behavior of Fe-Au systems under pressure. The speed of elastic waves propagating through a material is a measurable property of condensed matter that is easily matched with seismic or experimental data when modeling the Earth's interior. Using Navier's relation (49, 50), we mapped the elastic properties space of the Fe-Au phases predicted in

this study into longitudinal (v_l), transverse (v_t), and average (v_m) elastic wave speeds. These speeds are:

$$v_t = \sqrt{\frac{G}{\rho}}, \quad [2]$$

$$v_l = \sqrt{\frac{3B + 4G}{3\rho}}, \quad [3]$$

and

$$v_m = \left[\frac{1}{3} \left(\frac{2}{v_t^3} + \frac{1}{v_l^3} \right) \right]^{\frac{1}{3}}, \quad [4]$$

where B and G are the bulk and shear modulus, respectively, and ρ is the density of the material. The average wave speed is reported as the speed of sound (v_s) in Table 2. The v_s therefore captures the elastic anisotropy and, by extension, sound wave anisotropy in the system, should it exist.

Compounds in the Earth's interior each have different densities and sound speeds; thus, these values can be used in conjunction with seismic data to provide insight on its composition (15, 51–53). Seismological studies (18) suggest that the Earth's core must include some light siderophile elements to explain its lower density than that of pure Fe (19–22). In addition to having a higher density, hcp-Fe has a much higher velocity of sound than predicted from models of the core, as shown in Table 2. While introducing light elements, as in Fe₆₂C₂ and Fe₆₀C₄ (48), improves agreement with the PREM density, it does so at the expense of worsening agreement in the sound speed.

The extracted density and sound speeds for the Pmmn-AuFe₄ and I4/m-AuFe₃ phases are also reported in Table 2. The Cmcm-AuFe₄ phase was not included because the pressure at which we are making this comparison is outside the stability range of this phase (Fig. 1c). Compared with hcp-Fe or other Fe-rich model structures (Fe₆₂C₂ or Fe₆₀C₄) (48), Pmmn-AuFe₃ and I4/m-AuFe₄ have average sound speeds that are very much closer to that from the PREM model (15). Particularly, the metastable Pmmn-AuFe₃ phase has v_s that is closest to the PREM's, further supporting the stabilization of the Pmmn-AuFe₃ over the I4/m-AuFe₄ at the Earth's core's (> 2000 K) temperature. However, the densities of Pmmn-AuFe₄ and I4/m-AuFe₃ are significantly higher than both hcp-Fe and the PREM model data. The results suggest that combining Fe and Au with Ni or other light elements to form ternary systems could yield calculated densities and sound speeds closer to the PREM data (54). Overall, the addition of Au to the base Fe leads to a decrease in seismic velocities towards the geophysical observations at the CMB and the outer core. We opine that, if Au is present, the Fe content that will be required to match precisely the Earth's core profile would be less than what is required in the light-element-Fe alloys (48).

Implications for thermal conductivity at the CMB. The thermal conductivities of the Earth's lower mantle and core greatly impact convection dynamics. They also determine the ease of heat transport from the core to the mantle, thereby maintaining the heat energy budget for the Earth's geodynamo. As a result, there is a large body of work investigating thermal properties of iron and its alloys within a pressure-temperature regime relevant to the silicate mantle and core (55–57). Meanwhile, direct measurement of thermal conductivity under such extreme conditions still poses formidable challenges, so estimation of thermal conductivities from first-principles electronic structure calculations must suffice. Thus, identifying alloys and compounds of Fe with potentially high thermal conductivity is interesting as they could facilitate thermal convection at both the core-mantle boundary (CMB) and the inner-core boundary (ICB).

The coupling between mobile electrons and lattice vibrations dominates the heat transfer process of metals. The Wiedemann-Franz law (58) describes the relationship between electronic thermal conductivity and electrical resistivity as:

$$k = \frac{LT}{\varrho}, \quad [5]$$

where $L = 2.44 \times 10^{-8} W\Omega/K^2$ is the Lorentz number, T is the absolute temperature, and ϱ is the electrical resistivity. Thus, calculation of the electronic thermal conductivity of Fe-Au compounds is dependent on the knowledge of their electrical resistivity, which is scarce in the literature, especially for newly synthesized or predicted materials, and its determination falls beyond the scope of this paper. However, the Wiedemann-Franz law is a lower bound for the total thermal conductivity in a metal (56). While the addition of the electronic contribution would help to quantitatively estimate the total thermal conductivity of the Fe-Au systems, calculation of the total phonon thermal conductivity (including both acoustic and optical processes) gives a reasonable description of the heat transport mechanism (56).

The total phonon thermal conductivity (k_{ph}) in the predicted Fe-Au compounds could be as high as 68 W/mK in Pmmn-AuFe₃ at 200 GPa and room temperature, and as low as 5.2 W/mK in I4/m-AuFe₄ at 200 GPa and 2500 K (Fig. 5a). Notably, the thermal conductivity of the CMB, corresponding to 136 GPa and 3750 K, is reported to be 90 W/mK (56). The pressure regime where Cmcmm-AuFe₄ is stable is therefore most representative of the CMB. Cmcmm-AuFe₄ has a k_{ph} of 6 W/mK at 140 GPa and 3100 K. The k_{ph} of the Cmcmm-AuFe₄ corresponds to 6.7% of the total thermal conductivity of the CMB. Given that the reported thermal conductivity in Ref. (56) already captured the electronic and vibrational contributions to the thermal conductivity (as well as those from any impurities), it then implies that the phonon process is significant in the Fe-Au compounds during heat transport at the CMB. Excess heat that is not transported by the mantle- or CMB-bound Fe-Au compounds is, instead, transported through compositional convection into the inner core (56). Unreacted Au, if available, may be transported through this process into the solid Earth's inner core to form other stable Fe-Au compounds, such as Pmmn-AuFe₃ and I4/m-AuFe₄.

CONCLUSION

In this work, we investigated the possible formation of stable Fe-Au compounds under pressure using density-functional methods. We found that, at high pressure, Au forms several stable compounds with Fe, which has strong implication for understanding the form that Au may take in the Earth's mantle, CMB, and beyond. The Fe-Au intermetallic compounds are predicted to be stabilized by high pressure and electron transfer. Au exists as an anion in AuFe₃ and as cation in two AuFe₄ polymorphs, providing further evidence to support the striking chemistry of Au being able to adopt variable oxidation states at high pressure. At 140 GPa, Au attains a magnetic moment of $0.52\mu_B$ in Cmcmm-AuFe₄, making it ferromagnetic in nature. The speed of sound calculated for the various Fe-Au phases shows lower deviation from the PREM data compared to the other Fe-light element models compared. Furthermore, the computed thermal conductivity data for the various Fe-Au compounds shows that Fe-Au compounds have significant lattice thermal conductivity. This suggests that, beyond electronic phenomenon, the lattice vibrations also contribute to heat transport within the Earth's core and at the CMB. The results from this study show that some part of the depleted Au could be mixed with Fe in the CMB and the outer region of the core. As such, our Fe-Au model could serve to explain the seismological structure of the upper part of the Earth's interior, up to the core-mantle boundary, and some part of the outer core. Our work has strong implications for geoscience in the area of the Earth's magnetic field and could be extended to study how Au is stored in the Earth's solid, ferric inner core at pressures above 300 GPa.

MATERIALS AND METHODS

The crystal structure search was carried out using the particle swarm-intelligence optimization (PSO) algorithm using the Calypso program (59, 60). The structure search was performed for pressures of 0, 50, 100, 140, and 200 GPa, with simulation cells containing 1-4 formula units of Fe_xAu_y. The stability of various phases with respect to decomposition was assessed by constructing their convex hull. Electronic structure calculations for structural optimization and property evaluations were performed with density-functional theory (DFT) and dynamic stability calculations with density-functional perturbation theory (DFPT) (61) as implemented in the Vienna Ab initio Simulation Package (VASP) (62) code. These calculations used the projector-augmented wave (PAW) (63) approach, in which the valence states of Au and Fe were treated as $5d^{10}6s^1$ and $3p^63d^74s^1$, respectively. The Perdew-Burke-Ernzerhof (PBE) (64) generalized gradient approximation (GGA) functional was selected and the planewave energy cut-off was set to 450 eV. The GGA+*U* framework was used to apply an on-site Coulomb interaction to improve treatment of the 3d electrons of Fe. The Hubbard *U* parameter was set to 8.6 eV (65, 66) and such treatment of Fe has previously shown good agreement with experimental results (67) over the pressure range of interest. To ensure that forces on all atoms were converged to within 1 meV/Å, the Monkhorst-Pack scheme was used to sample the Brillouin zone, with a **k** spacing of $2\pi \times 0.02 \text{ \AA}^{-1}$. Dynamical calculations for the thermal properties were carried out using the Quantum Espresso (QE) code (68), again with the PBE+*U* exchange-correlation functional. Well converged total energies were obtained using a planewave

kinetic-energy cut-off of 150 Ry and Monkhorst-Pack \mathbf{k} -point meshes of $9 \times 9 \times 3$ and $8 \times 8 \times 8$ for AuFe₃ and AuFe₄, respectively.

To predict the thermal conductivity, the ShengBTE code (69) was used to iteratively solve the Boltzmann Transport Equation (BTE):

$$F_\lambda = \tau_\lambda^0 (V_\lambda + \Delta_\lambda). \quad [6]$$

Here, F_λ is the generalized mean free path, τ_λ^0 is the relaxation time of mode λ in the relaxation time approximation (RTA), and Δ_λ gives the deviation of the solution from the RTA. The phonon assisted thermal conductivity (k_{ph}) tensor can then be obtained as

$$k_{\text{ph}}^{\alpha\beta} = \frac{1}{k_B T^2 \Omega N} \sum_\lambda n^0 (n^0 + 1) (\hbar \omega_\lambda)^2 v_{\alpha,\lambda} v_{\beta,\lambda}, \quad [7]$$

where α and β are the three coordinate directions (x , y , and z). k_B , T , Ω , and N are Boltzmann's constant, the temperature, the unit-cell volume, and the number of \mathbf{q} -points in the integral over the BZ, respectively. The sum runs over all the phonon modes λ , \hbar is the reduced Planck constant, and ω_λ is the phonon frequency. For the first iteration step, Δ_λ is set to zero, which is equivalent to starting the iterative procedure from the RTA solution. The solution is converged when the relative change in all the components of the thermal conductivity tensor becomes smaller than 10^{-5} W/mK. To solve the BTE, we used a $4 \times 4 \times 1$ supercell to calculate the third-order interatomic force constants (IFCs) for the Pmmn and Cmcmm phases, and a $3 \times 3 \times 3$ supercell for the I4/m phase. The force cut-off distance was set such that the interaction range includes the five nearest neighbors for AuFe₃ and the three nearest neighbors for AuFe₄. Meshes of $7 \times 7 \times 5$ and $5 \times 5 \times 5$ \mathbf{q} -points were used to calculate the second-order IFCs needed to compute the k_{ph} of AuFe₃ and AuFe₄, respectively.

Data Availability. All study data are included in the article and/or SI Appendix.

Supporting Information Appendix (SI). The supporting information contains additional computational results, including plots of the zero-point energy (ZPE)-corrected convex hull, equation of states, 2D-projected crystal structures with Bader charge distributions, thermal conductivity at 300 K, electronic band structures, projected electronic density of states, vibrational entropies evolution with temperature, elastic modulus data and atomic charge distributions.

ACKNOWLEDGMENTS. A.A.A. and E.R.J acknowledge the support by the Natural Sciences and Engineering Research Council of Canada (NSERC). Computing resource is provided by Lawrence Livermore National Laboratory, Westgrid, and Compute Canada.

References.

- Bernard J Wood, Michael J Walter, and Jonathan Wade. Accretion of the earth and segregation of its core. *Nature*, 441(7095):825–833, 2006.
- DJ Stevenson. Models of the earth's core. *Science*, 214(4521):611–619, 1981.
- Robert Sprague Jones. *Gold in Meteorites and in the Earth's Crust*, volume 603. US Government Printing Office, 1968.
- William J McDonough and S-S Sun. The composition of the earth. *Chemical Geology*, 120(3-4):223–253, 1995.
- Thomas J Ahrens. *Global earth physics: a handbook of physical constants*, volume 1. American Geophysical Union, 1995.
- George R Helffrich and Bernard J Wood. The earth's mantle. *Nature*, 412(6846):501–507, 2001.
- Douglas R McKay and Daniel A Peters. The midas touch: Gold and its role in the global economy. *Plastic Surgery*, 25(1):61–63, 2017.

- R Briggs, F Coppari, MG Gorman, RF Smith, SJ Tracy, AL Coleman, A Fernandez-Pañella, M Millot, JH Eggert, and DE Fratanduono. Measurement of body-centered cubic gold and melting under shock compression. *Physical Review Letters*, 123(4):045701, 2019.
- Leonid Dubrovinsky, Natalia Dubrovinskaia, Wilson A Crichton, Arkady S Mikhaylushkin, Sergey I Simak, Igor A Abrikosov, J Souza de Almeida, Rajeev Ahuja, Wei Luo, and Börje Johansson. Noblest of all metals is structurally unstable at high pressure. *Physical Review Letters*, 98(4):045503, 2007.
- Takahiro Ishikawa, Kuniko Kato, Masaya Nomura, Naoshi Suzuki, Hitose Nagara, and Katuya Shimizu. Pressure-induced stacking sequence variations in gold from first principles. *Physical Review B*, 88(21):214110, 2013.
- Rajeev Ahuja, Sandeep Reki, and Börje Johansson. Theoretical prediction of a phase transition in gold. *Physical Review B*, 63(21):212101, 2001.
- Per Söderlind. Comment on "theoretical prediction of phase transition in gold". *Physical Review B*, 66(17):176201, 2002.
- JC Boettger. Theoretical extension of the gold pressure calibration standard beyond 3 mbars. *Physical Review B*, 67(17):174107, 2003.
- John T Wasson. *Meteorites: their record of early solar-system history*. New York: Freeman, 1985.
- Adam M Dzewonski and Don L Anderson. Preliminary reference earth model. *Physics of the Earth and Planetary Interiors*, 25(4):297–356, 1981.
- Hrvoje Tkalić and Thanh-Son Phạm. Shear properties of earth's inner core constrained by a detection of j waves in global correlation wavefield. *Science*, 362(6412):329–332, 2018.
- C Ashley Norris and Bernard J Wood. Earth's volatile contents established by melting and vaporization. *Nature*, 549(7673):507–510, 2017.
- Agnes Dewaele, Paul Loubeyre, Florent Occelli, Mohamed Mezouar, Peter I Dorogokupets, and Marc Torrent. Quasihydrostatic equation of state of iron above 2 mbar. *Physical Review Letters*, 97(21):215504, 2006.
- Claude J Allegre, Jean-Paul Poirier, Eric Humler, and Albrecht W Hofmann. The chemical composition of the earth. *Earth and Planetary Science Letters*, 134(3-4):515–526, 1995.
- Adebayo A Adeleke and Yansun Yao. Formation of stable compounds of potassium and iron under pressure. *Journal of Physical Chemistry A*, 124(23):4752–4763, 2020.
- Adebayo A Adeleke, Elissaios Stavrou, Adebayo O Adeniyi, Biao Wan, Huiyang Gou, and Yansun Yao. Two good metals make a semiconductor: A potassium-nickel compound under pressure. *Physical Review B*, 102(13):134120, 2020.
- Jean-Paul Poirier. Light elements in the earth's outer core: a critical review. *Physics of the Earth and Planetary Interiors*, 85(3-4):319–337, 1994.
- Elissaios Stavrou, Yansun Yao, Alexander F Goncharov, Sergey S Lobanov, Joseph M Zaug, Hanyu Liu, Eran Greenberg, and Vitali B Prakapenka. Synthesis of xenon and iron-nickel intermetallic compounds at earth's core thermodynamic conditions. *Physical Review Letters*, 120(9):096001, 2018.
- Adebayo A Adeleke, Martin Kunz, Eran Greenberg, Vitali B Prakapenka, Yansun Yao, and Elissaios Stavrou. A high-pressure compound of argon and nickel: Noble gas in the earth's core? *ACS Earth and Space Chemistry*, 3(11):2517–2524, 2019.
- L Pleth Nielsen, Flemming Besenbacher, I Stensgaard, E Laegsgaard, C Engdahl, Per Stoltze, Karsten Wedel Jacobsen, and Jens Kehlet Nørskov. Initial growth of au on ni (110): Surface alloying of immiscible metals. *Physical Review Letters*, 71(5):754, 1993.
- S Mehendele, Y Girard, V Repain, C Chacon, J Lagoute, S Rousset, Madhura Marathe, and Shobhana Narasimhan. Ordered surface alloy of bulk-immiscible components stabilized by magnetism. *Physical Review Letters*, 105(5):056101, 2010.
- Xiao Dong, Artem R Oganov, Guangrui Qian, Xiang-Feng Zhou, Qiang Zhu, and Hui-Tian Wang. How do chemical properties of the atoms change under pressure. *arXiv preprint arXiv:1503.00230*, 2015.
- W Tang, E Sarville, and G Henkelman. A grid-based bader analysis algorithm without lattice bias. *Journal of Physics: Condensed Matter*, 21(8):084204, 2009.
- Martin Jansen. The chemistry of gold as an anion. *Chemical Society Reviews*, 37(9):1826–1835, 2008.
- Ju Wei Shih. Magnetic properties of gold-iron alloys. *Physical Review*, 38(11):2051, 1931.
- AR Kaufmann, ST Pan, and JR Clark. Magnetization of gold-iron and gold-nickel solid solutions. *Reviews of Modern Physics*, 17(1):87, 1945.
- ST Pan, AR Kaufmann, and F Bitter. Ferromagnetic gold-iron alloys. *Journal of Chemical Physics*, 10(6):318–321, 1942.
- A Stamatelatos, P Pouloupoulos, A Goschew, P Fumagalli, E Sarigiannidou, L Rapenne, Christine Opagiste, S Grammatikopoulos, F Wilhelm, and A Rogalev. Paramagnetic gold in a highly disordered Au-Ni-O alloy. *Scientific Reports*, 9(1):1–8, 2019.
- JX Zheng-Johansson, O Eriksson, B Johansson, L Fast, and R Ahuja. Comment on "stability and the equation of state of α -manganese under ultrahigh pressure". *Physical Review B*, 57(17):10989, 1998.
- Wilhelm Blitz, Friedrich Weibke, Versuchen Hans-Joachim Ehrhorn, Roman Wedemeyer, and Friedrich Weibke. Über wertigkeit und chemische kompression von metallen in verbindung mit gold. *Zeitschrift für anorganische und allgemeine chemie*, 236(1):12–23, 1938.
- RA Sperl, PR Gil, F Zhang, M Zanella, and WJ Parak. Gold: Chemistry, materials and catalysis issue. *Chemical Society Review*, 37(9):1909–1930, 2008.
- Brian J Corden, James A Cunningham, and Richard Eisenberg. Crystal and molecular structure of tris (tetra-n-butylammonium) octacyanomolybdate (v). *Inorganic Chemistry*, 9(2):356–362, 1970.
- Logan K Magad-Weiss, Adebayo A Adeleke, Eran Greenberg, Vitali B Prakapenka, Yansun Yao, and Elissaios Stavrou. High-pressure structural study of α -mn: Experiments and calculations. *Physical Review B*, 103(1):014101, 2021.
- M Born and K Huang. Theory of crystal lattices, clarendon, 1956.
- Richard Hill. The elastic behaviour of a crystalline aggregate. *Proceedings of the Physical Society. Section A*, 65(5):349, 1952.
- Rodney Hill. Elastic properties of reinforced solids: some theoretical principles. *Journal of the Mechanics and Physics of Solids*, 11(5):357–372, 1963.
- Félix Mouhat and François-Xavier Coudert. Necessary and sufficient elastic stability condi-

- tions in various crystal systems. *Physical Review B*, 90(22):224104, 2014.
43. Pasquale Pavone, Stefano Baroni, and Stefano de Gironcoli. $\alpha \leftrightarrow \beta$ phase transition in tin: A theoretical study based on density-functional perturbation theory. *Physical Review B*, 57(17):10421, 1998.
 44. John M Ziman. *Electrons and phonons: the theory of transport phenomena in solids*. Oxford university press, 2001.
 45. Zhi Guo, Amit Verma, Xufei Wu, Fangyuan Sun, Austin Hickman, Takekazu Masui, Akito Kuramata, Masataka Higashiwaki, Debdeep Jena, and Tengfei Luo. Anisotropic thermal conductivity in single crystal β -gallium oxide. *Applied Physics Letters*, 106(11):111909, 2015.
 46. Ankit Jain and Alan JH McGaughey. Thermal conductivity of compound semiconductors: Interplay of mass density and acoustic-optical phonon frequency gap. *Journal of Applied Physics*, 116(7):073503, 2014.
 47. Ruiqiang Guo, Xinjiang Wang, and Baoling Huang. Thermal conductivity of skutterudite CoSb_3 from first principles: substitution and nanoengineering effects. *Scientific Reports*, 5(1):1–9, 2015.
 48. Yunguo Li, Lidunka Vočadlo, and John P Brodholt. The elastic properties of hcp-Fe alloys under the conditions of the earth's inner core. *Earth and Planetary Science Letters*, 493:118–127, 2018.
 49. Orson L Anderson. A simplified method for calculating the debye temperature from elastic constants. *Journal of Physics and Chemistry of Solids*, 24(7):909–917, 1963.
 50. Edward Schreiber, Orson L Anderson, Naohiro Soga, and James F Bell. Elastic constants and their measurement. 1975.
 51. Lidunka Vočadlo. Ab initio calculations of the elasticity of iron and iron alloys at inner core conditions: Evidence for a partially molten inner core? *Earth and Planetary Science Letters*, 254(1-2):227–232, 2007.
 52. Anastasia P Kantor, Innokenty Yu Kantor, Alexander V Kurnosov, Alexei Yu Kuznetsov, Natalia A Dubrovinskaia, Michael Krisch, Alexei A Bossak, Vladimir P Dmitriev, Vadim S Urusov, and Leonid S Dubrovinsky. Sound wave velocities of fcc Fe–Ni alloy at high pressure and temperature by mean of inelastic X-ray scattering. *Physics of the Earth and Planetary Interiors*, 164(1-2):83–89, 2007.
 53. Jin Liu, Jung-Fu Lin, Ahmet Alatas, and Wenli Bi. Sound velocities of bcc-Fe and $\text{Fe}_{0.85}\text{Si}_{0.15}$ alloy at high pressure and temperature. *Physics of the Earth and Planetary Interiors*, 233:24–32, 2014.
 54. Yu He, Shichuan Sun, Duck Young Kim, Bo Gyu Jang, Heping Li, and Ho-kwang Mao. Superionic iron alloys and their seismic velocities in earth's inner core. *Nature*, 602(7896):258–262, 2022.
 55. Wenjun Yong, Richard A Secco, Joshua AH Littleton, and Reynold E Silber. The iron invariance: implications for thermal convection in earth's core. *Geophysical Research Letters*, 46(20):11065–11070, 2019.
 56. Hitoshi Gomi, Kenji Ohta, Kei Hirose, Stephane Labrosse, Razvan Caracas, Matthieu J Verstraete, and John W Hernlund. The high conductivity of iron and thermal evolution of the earth's core. *Physics of the Earth and Planetary Interiors*, 224:88–103, 2013.
 57. Nico de Koker, Gerd Steinle-Neumann, and Vojtěch Vlček. Electrical resistivity and thermal conductivity of liquid Fe alloys at high P and T, and heat flux in earth's core. *Proceedings of the National Academy of Sciences*, 109(11):4070–4073, 2012.
 58. Orson L Anderson. The Grüneisen parameter for iron at outer core conditions and the resulting conductive heat and power in the core. *Physics of the Earth and Planetary Interiors*, 109(3-4):179–197, 1998.
 59. Yanchao Wang, Jian Lv, Li Zhu, and Yanming Ma. Crystal structure prediction via particle-swarm optimization. *Physical Review B*, 82(9):094116, 2010.
 60. Yanchao Wang, Jian Lv, Li Zhu, and Yanming Ma. Calypso: A method for crystal structure prediction. *Computer Physics Communications*, 183(10):2063–2070, 2012.
 61. Stefano Baroni, Stefano De Gironcoli, Andrea Dal Corso, and Paolo Giannozzi. Phonons and related crystal properties from density-functional perturbation theory. *Reviews of Modern Physics*, 73(2):515, 2001.
 62. Georg Kresse and Jürgen Hafner. Ab initio molecular dynamics for liquid metals. *Physical Review B*, 47(1):558, 1993.
 63. Georg Kresse and Daniel Joubert. From ultrasoft pseudopotentials to the projector augmented-wave method. *Physical Review B*, 59(3):1758, 1999.
 64. John P Perdew, Kieron Burke, and Matthias Ernzerhof. Generalized gradient approximation made simple. *Physical Review Letters*, 77(18):3865, 1996.
 65. Matteo Cococcioni and Stefano De Gironcoli. Linear response approach to the calculation of the effective interaction parameters in the LDA+U method. *Physical Review B*, 71(3):035105, 2005.
 66. Arnab Majumdar, S Tse John, Min Wu, and Yansun Yao. Superconductivity in Fe₅. *Physical Review B*, 96(20):201107, 2017.
 67. HK Mao, Y Wu, LC Chen, JF Shu, and Andrew P Jephcoat. Static compression of iron to 300 GPa and $\text{Fe}_{0.8}\text{Ni}_{0.2}$ alloy to 260 GPa: Implications for composition of the core. *Journal of Geophysical Research: Solid Earth*, 95(B13):21737–21742, 1990.
 68. Paolo Giannozzi, Stefano Baroni, Nicola Bonini, Matteo Calandra, Roberto Car, Carlo Cavazzoni, Davide Ceresoli, Guido L Chiarotti, Matteo Cococcioni, Ismaila Dabo, et al. QUANTUM ESPRESSO: a modular and open-source software project for quantum simulations of materials. *Journal of Physics: Condensed Matter*, 21(39):395502, 2009.
 69. Wu Li, Jesús Carrete, Nebil A Katcho, and Natalio Mingo. Shengbte: A solver of the boltzmann transport equation for phonons. *Computer Physics Communications*, 185(6):1747–1758, 2014.